Scaling in plasticity-induced cell-boundary microstructure: Fragmentation and rotational diffusion

Scaling in plasticity-induced cell-boundary microstructure: Fragmentation and rotational diffusion

James P. Sethna and Valerie R. Coffman
Laboratory of Atomic and Solid State Physics (LASSP), Clark Hall, Cornell University, Ithaca, New York 14853-2501, USA

Eugene Demler
Physics Department, Lyman Labs, Harvard University, Cambridge, Massachusetts 02138, USA

(Received 3 October 2002; revised manuscript received 5 February 2003; published 27 May 2003)

We develop a simple computational model for cell-boundary evolution in plastic deformation. We study the cell-boundary size distribution and cell-boundary misorientation distribution that experimentally have been found to have scaling forms that are largely material independent. The cell division acts as a source term in the misorientation distribution which significantly alters the scaling form, giving it a linear slope at small misorientation angles as observed in the experiments. We compare the results of our simulation with two closely related exactly solvable models that exhibit scaling behavior at late times: (i) fragmentation theory and (ii) a random walk in rotation space with a source term. We find that the scaling exponents in our simulation agree with those of the theories, and that the scaling collapses obey the same equations, but that the shape of the scaling functions depends upon the methods used to measure sizes and to weight averages and histograms.

DOI: 10.1103/PhysRevB.67.184107 PACS number(s): 61.72.Lk, 61.72.Mm, 62.20.Fe

I. INTRODUCTION

After significant plastic deformation, the dislocation tangles in crystals often organize themselves into sharp walls separating nearly dislocation-free cells; the crystallographic axes rotate slightly across each cell boundary. These cells undergo refinement (become smaller) under increased deformation, and recent experiments[1,2] indicate that both the misorientation angles and the cell sizes have power-law scaling with material-independent scaling forms for the probability distributions. We introduce here a simple model of cell division and rotational diffusion which exhibits this type of scaling, and which provides insights into the origins for the experimental scaling distributions. In particular, we argue that cell division (driving the refinement) is responsible for the linear growth of the misorientation scaling distribution at small angles.

Cell boundaries are distinct from grain boundaries in that their misorientation angle across them is small (at most a few degrees) and they form in a nonequilibrium process, typically at temperatures where diffusion is not relevant (so, for example, the impurity segregation characteristic of many grain boundaries is not observed at cell boundaries). As deformation proceeds, the cell structure refines (the average cell size L_{av} becomes smaller), and the average cell misorientation angle θ_{av} grows.

The cell boundaries are separated into into two classes. An early work[3] called them ''ordinary cell walls'' and ''dense dislocation walls''; later authors[1] have called them GNB's (''geometrically necessary boundaries'') and IDB's (''incidental dislocation boundaries''). The GNB's typically align roughly parallel to one another, have larger misorientation angles, and are longer, often forming the boundaries of two or more cells.

(The term ''geometrically necessary'' is unfortunate. Geometrically necessary *dislocations* are those required to mediate macroscopic strain gradients and rotation gradients, as distinguished from geometrically unnecessary dislocations whose Burgers vectors cancel out on long length scales. All cell walls are associated with small relative rotations between cells, and are hence composed of geometrically necessary dislocations on scales comparable to the cell sizes. On longer scales, far from building up large macroscopic rotations, the rotations mediated by neighboring geometrically necessary *boundaries* tend to cancel,[4] leading to little or no long-range rotation gradient. Hence, as cell boundaries, the GNB's are most akin to the geometrically unnecessary dislocations.)

Hughes *et al.*[1,2] studied the distribution functions for these two types of cell walls, and found a simple scaling behavior, largely independent of material. In particular, for the GNB's $\theta_{av} \sim \epsilon^{2/3}$ and $L_{av} \sim \epsilon^{-2/3}$, while for the IDB's $\theta_{av} \sim \epsilon^{1/2}$ and $L_{av} \sim \epsilon^{-1/2}$, where ϵ is the magnitude of the net plastic strain. Moreover, data for several materials and different strain amplitudes all collapse onto apparently universal scaling curves $\rho_{\rm mis}$ and $\rho_{\rm size}$ when rescaled to the average angle:

$$\rho(\theta) = \theta_{av}^{-1} \rho_{\rm mis}(\theta/\theta_{av}) \tag{1}$$

and

$$\rho(L) = L_{av}^{-1} \rho_{\rm size}(L/L_{av}). \tag{2}$$

We will study the scaling of these probability distributions $\rho(\theta)$ and $\rho(L)$ using a simple model.

II. MODEL

How much of this apparently universal behavior can be captured in a simple model of cell rotation and refinement? The model we propose is one in which cells become smaller by subdivision (leading to a fragmentation theory for the size distribution), and undergo random angular reorientations as the strain increases. Our model does not incorporate the anisotropy in the external strain field, and so has nothing to say

about how cell structure morphology might change, say, between tensile and rolling deformation or as the crystalline orientation changes. One should view our model as a caricature of the real system; our results suggest that the experimentally observed scaling behavior may be generic to any microscopic mechanism which fragments and randomly reorients cells.

Our computational model starts with one large cubical cell. We assume a cubic crystal, with initial crystalline axes aligned with the axes of our cube, so the initial orientation is described by a rotation matrix $R(0)$ equal to an identity matrix. The dynamics of our model incorporates two pieces; rotational diffusion and cell splitting events.

Rotational diffusion. The orientation of each cell α undergoes a simple random walk in rotation angle space, with strain increments playing the role of the time step. It is convenient to write the current orientation $R_\alpha(t)=\exp(\mathbf{n}\cdot\mathbf{J})$, where the matrix $\mathbf{J}_i=\boldsymbol{\epsilon}_{ijk}$ (with $\boldsymbol{\epsilon}_{ijk}$ the totally antisymmetric tensor) generates an infinitesimal rotation about the ith axis. Since the cell-boundary misorientation angles experimentally are small (around a degree or so), we may expand the exponential in this expression,

$$R=\exp(\mathbf{n}\cdot\mathbf{J})\simeq\begin{pmatrix} 1-\frac{n_2^2+n_3^2}{2} & n_3 & -n_2 \\ -n_3 & 1-\frac{n_1^2+n_3^2}{2} & n_1 \\ n_2 & -n_1 & 1-\frac{n_1^2+n_2^2}{2} \end{pmatrix}. \tag{3}$$

(Large-angle corrections are discussed in Refs. 5 and 6.) In this approximation, diffusion in the manifold of crystalline orientations can be written as an ordinary diffusion equation in the three-dimensional coordinate $\mathbf{n}$. If we assume $\boldsymbol{\epsilon}(t)$ is a monotonically increasing strain, then the three-dimensional probability distribution of grain orientations $\Lambda(\mathbf{n})$ evolves according to the equation

$$\partial\Lambda(\mathbf{n})/\partial\boldsymbol{\epsilon}=-D\nabla^2\Lambda(\mathbf{n}), \tag{4}$$

where D is the "orientational diffusion constant" and the Laplacian $\nabla^2=\partial^2/\partial n_x^2+\partial^2/\partial n_y^2+\partial^2/\partial n_z^2$, The random walk described by this diffusion equation is implemented numerically by adding a Gaussian random vector to $\mathbf{n}$ with components of root-mean-square length $\sqrt{2D\Delta\boldsymbol{\epsilon}}$, whenever the strain for the cell is incremented by $\Delta\boldsymbol{\epsilon}$.

Cell splitting events. Our model, for simplicity, divides cells only along planes perpendicular to one of the crystalline axes. Thus, our cell structure is composed of rectangular parallelepipeds. The rate of cell division in our model depends only on the current size and shape of the cell, and not on its environment. There are several different physical mechanisms that might be responsible for cell division. Broadly speaking, we classify them by dimensional analysis: there are mechanisms that divide cells at a rate proportional to their current volume V, their current surface area S, their current perimeter P, or at a uniform rate independent of the current size $U=1$. Once a cell has been chosen to split, we must choose an axis and a position along that axis to place the new cell wall. To keep our aspect ratios reasonable, we have chosen the probability of splitting along a given axis proportional to the length of the cell along that axis. The position of the new cell wall along the split axis is chosen randomly in all cases. The two cells formed by splitting inherit their parent's orientation: the new cell walls thus start out at zero misorientation angle, which will be important when we study the misorientation angle distribution.

Our model for cell splitting is closely related to a well-studied model of fragmentation.[7,8] In fragmentation theory, the splitting rate is assumed a function of the volume, so, for example, a cell of volume V could fracture with a rate AV^γ. In our problem, $\gamma=0$ and $\gamma=1$ correspond precisely to uniform and volume cell splitting rates, while $\gamma=1/3$ and $\gamma=2/3$ approximately correspond to perimeter and area splitting. The evolution law in fragmentation theory corresponding to our model is easily seen to be[8]

$$\partial c(V,\boldsymbol{\epsilon})/\partial\boldsymbol{\epsilon}=-AV^\gamma c(V,\boldsymbol{\epsilon})+2\int_V^\infty A\tilde{V}^{\gamma-1}c(\tilde{V},\boldsymbol{\epsilon})d\tilde{V}, \tag{5}$$

where c is the concentration of fragments with volume V. To relate this to experimental measurements [Eq. (2)], which produce probability distributions of lengths rather than concentrations of volumes, we can change variables from V to $L=V^{1/3}$. The probability distribution of lengths with all cells weighted uniformly is

$$\rho(L)=\frac{3L^2c(L^3,\boldsymbol{\epsilon})}{\int_0^\infty c(V,\boldsymbol{\epsilon})dV}. \tag{6}$$

The histograms produced by our simulations are a result of three choices. First, there is a choice in how we define the size (length L) of the cell. In computing the averages and histograms from the simulation data, we typically define the size of a cell to be its length along any one of the axes: all three lengths are incorporated into the averages and histograms. This definition of size corresponds to that used in experiment. Alternatively, in order to compare the histograms from the simulation to fragmentation theory (which keeps track only of the volumes, not the shapes, of the cells), we can define the size of the cell as the cube root of the volume. Second, there is a choice in the splitting dynamics as discussed above: cells can divide at rates proportional to their volume, surface area, perimeter, or at a uniform rate. In fragmentation theory, the rate of splitting is proportional to V^γ as discussed below: thus fragmentation theory is exact for our simulation with volume splitting ($\gamma=1$) and uniform splitting rates ($\gamma=0$), but does not directly apply to the perimeter and surface simulations, whose splitting rates depend upon the shapes of the cells as well as their volumes. Finally, one must address how to weigh the contributions of different cells in the probability distribution. For example, an experiment that measures cell sizes by taking an XY cross section and then weighting each observed cell equally in the average is effectively weighting the three-dimensional cells

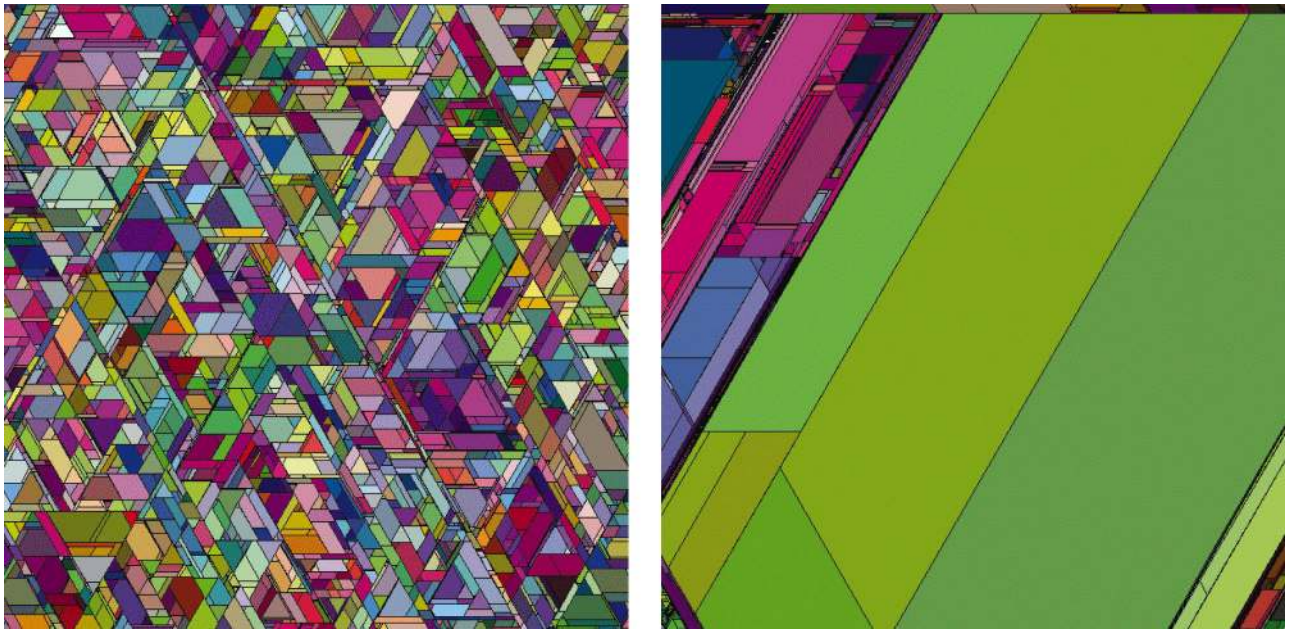

FIG. 1. (Color) Simulated cell morphologies: Diagonal cross section of the cell morphologies in two model simulations, in a central plane perpendicular to the 111 axis. Left: Area splitting rate. Right: Uniform splitting rate. The area splitting yields rather uniform cell sizes, while the uniform splitting yields an enormous range of cell sizes and a fractal morphology. The colors are chosen to represent the rotations of the crystalline axes of the individual grains. The original orientation $\mathbf{n}=0$ is colored medium gray. In grayscale, darker and lighter grays represent the magnitude of the deviation. In full color, n_x, n_y, and n_z are mapped, respectively, onto deviations in red, green, and blue with a scale-factor chosen to saturate at the largest rotations.

by their extent in the Z direction (roughly weighting each cell by its perimeter or by L). We compute the averages and histograms from the simulation data by weighting each cell uniformly or by its volume, surface area, or perimeter. We will soon see that the scaling exponents for the average size depend on only the splitting dynamics γ not on the measurement of size or the weight of the distribution. We will also see that the shape of the scaled probability distributions changes with different measurements of size or weights, but the distributions scale nonetheless.

If we define the size of the cell as the cube root of the volume, simulations that split cells at a uniform rate or at a rate proportional to the volume of the cell produce histograms that agree well with those given by fragmentation theory [Eq. (6)]. However, simulations that split cells at rates proportional to area and perimeter produce histograms that are shifted from Eq. (6). We focus here on the case where the rate is proportional to the surface area S of the cell (area) and the case where the rate is independent of the size and shape of the cell (uniform).

III. RESULTS

A. Morphologies

Figures 1 show the cell morphologies from the two simulations. Area splitting shows a fairly uniform density of cell sizes; this is characteristic also of the other size-dependent cell division rates. Uniform cell splitting rates produce a broad range of sizes: most cells are very small, so most cell divisions subdivide very small cells. Indeed, as we shall discuss below, the uniform model is at a critical point in fragmentation theory (the "shattering" transition[7]). Experimentally, there does not seem to be a consensus on whether the cell-size distribution is fractal[9] or whether it has a more traditional scaling distribution with a characteristic size that shrinks with time.[2]

B. Cell-size scaling

Figures 2 shows the mean cell size as it evolves with increasing strain in our model, under area splitting and random splitting. In the figure, we show a count average where each cell contributes equally, a perimeter average where cells are weighted by their perimeter, and area and volume average. Each of these has the size of the cell defined as the distance between parallel cell walls. The fourth average has the size defined as the cube root of the volume and is weighted uniformly.

The mean size for the cells in the area splitting model scales with $\epsilon^{-1/2}$. Assuming fragmentation theory [Eq. (5)] and scaling [Eq. (2), which can be derived from fragmentation theory[8] for $\gamma>0$], it is easy[10] to derive the power-law relation $L_{av}\sim\epsilon^{-1/3\gamma}$. Thus, the experimentally observed scaling of the IDB sizes suggests a cell splitting rate proportional to the cell surface area (left side of the figures), while the scaling $L_{\mathrm{av}}^{(GNB)}\sim\epsilon^{-2/3}$ of the GNB dislocations would suggest a mechanism with a cell splitting rate scaling as the cell volume to the 1/2 power. (See, however, Sec. IV A.)

Figures 3 show the histograms of cell sizes at the end of our simulation, with the five weights discussed above. Naturally, for example, if cells are weighted by their volume there is more weight in the histogram at larger sizes.

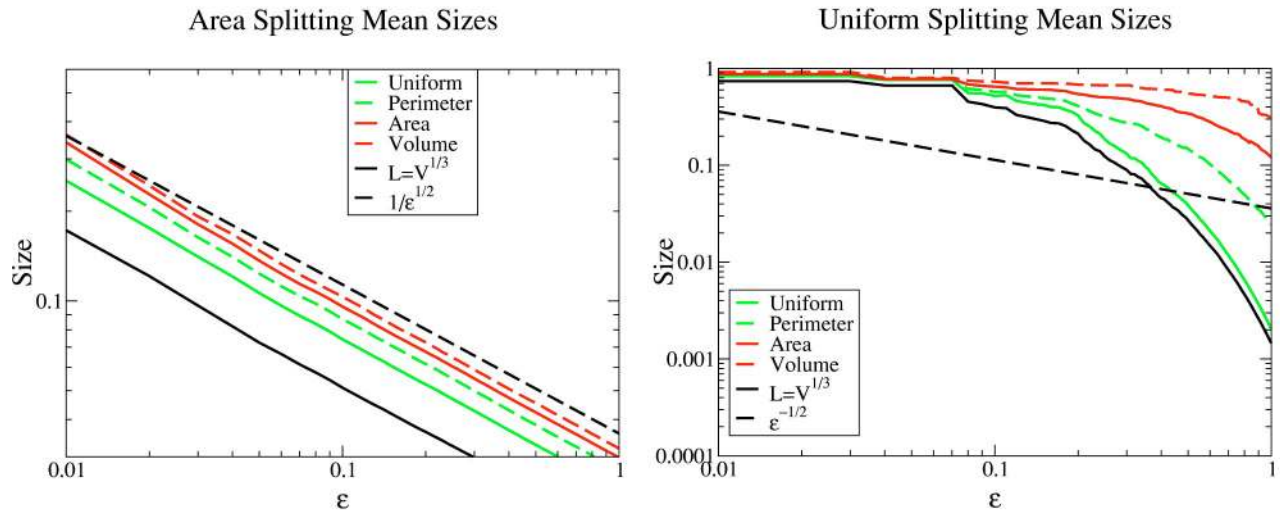

FIG. 2. Mean cell sizes versus strain: We measure the mean cell sizes, with each cell contributing to the average an amount given by volume, area, perimeter, or uniformly independent of its size. As noted in the text, the perimeter scaling corresponds effectively to a common experimental procedure of taking histograms. (Do not confuse, say, area weighted mean sizes and area weighted splitting rates. The different curves on each graph are different *measurements*, the different graphs are different *dynamics*.) We also include the mean size with the length measured as the cube root of the volume, with cells contributing uniformly, independent of their sizes. Left: Area splitting. The various measures are equivalent up to an overall scale factor for the model where the cell division rate is proportional to the surface area of the cells, and the cell size varies as $\epsilon^{-1/2}$. This equivalence is because the distribution of sizes is peaked about a typical size scales (Fig. 3), and can be derived from the scaling form for the cell-size distribution. Right: Uniform splitting. The various measures are very different for the case of random splitting, since the cell structures are fractal with cells of all sizes.

We first consider the left-hand panel, showing the simulation results with dynamics which split cells proportional to their surface area. The area splitting histograms, taken at different ϵ during our simulations, do indeed rapidly converge to those shown on the left panel of Fig. 3 [hence validating the scaling form equation (2)]. No matter how one defines the size L or how one weights the contribution of each cell, the histograms collapse onto scaling functions.

Fragmentation theory[8] calculates the scaling function explicitly that describes the distribution of sizes at late times. In particular, for area splitting ($\gamma=2/3$), the scaling function in Eq. (2) for a uniformly weighted distribution is,

$$\rho_{size}(x)=32x^2\exp(-4x^2/\pi)/\pi^2, \tag{7}$$

shown as the black, dashed line on the left in Fig. 3. As expected, it does indeed agree well with the size distribution

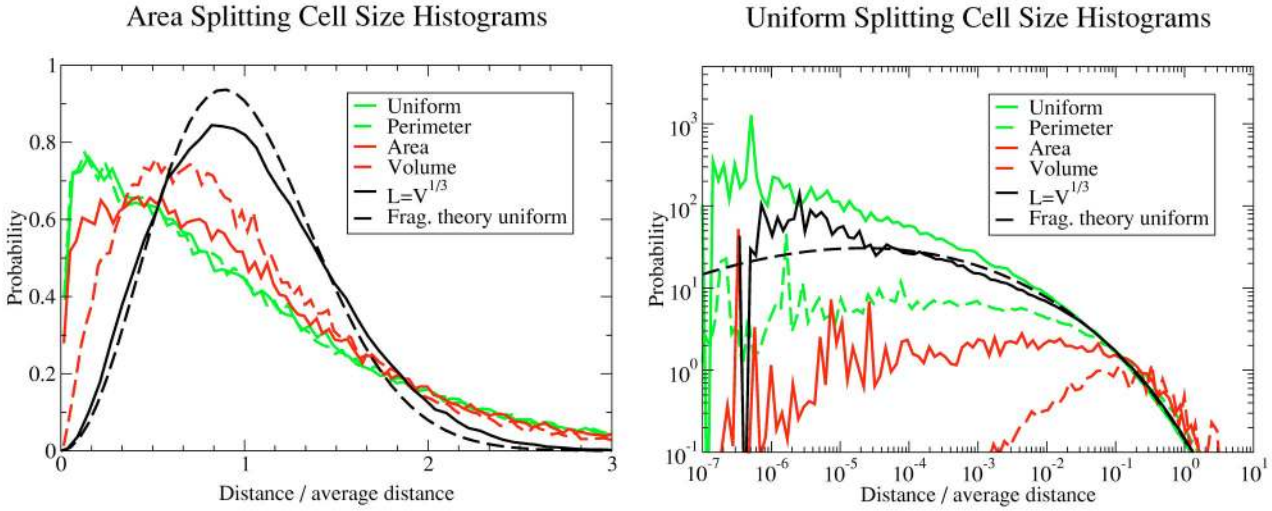

FIG. 3. Cell-size histogram: Histograms of cell sizes at the end of our simulation, rescaled to the average cell size (Fig. 2) according to Eq. (2). Again, there are different histograms depending upon how the cells are weighted in the average. Left: Area splitting. The black, dashed curve is the fragmentation theory prediction (Ref. 8) for the closely related problem where cells split at a rate proportional to volume $V^{2/3}$. Right: Uniform splitting. Notice that most of the cells (counted) are very small.

where L is defined as the cube root of the volume. The shift between these two curves is due to the difference in dynamics: our simulation splits cells at a rate proportional to the actual area of the cell, not by $V^{2/3}$. For volume splitting, with L defined as the cube root of the volume, the histograms from the simulation agree with those from fragmentation theory as expected.

The histograms that measure the length, width, and height of each cell are broader than those that measure the cube root of the volume. Cells with large aspect ratios will contribute one or two dimensions that are smaller than the cube root of volume and one or two that are larger. Notice that in Fig. 3 the cell-size probability density does not vanish at zero size L except for statistical weightings that involve the total volume. In our model, a subdivision occurs with equal probability at all thicknesses, so the probability density at zero thickness is finite. If the weights of the cells in the average is by the total volume, of course, then the thin cells contribute vanishing weight so the histogram goes to zero.

Consider now the right-hand panel of Fig. 3, with simulation results for dynamics which split cells at a uniform rate independent of their size. Notice first that the scales are logarithmic. There is an enormous range of cell sizes, with peak probabilities (by most measures) at very small sizes. The uniform splitting model is at a critical point in the parameter $\gamma=0$, the *shattering transition*,[7] beyond which ($\gamma<0$) there an infinite dust of zero-size particles. At this critical point, there are exact solutions for the cell-size distribution (black, dashed curve shown in Fig. 3, to be compared with the $L=V^{1/3}$ simulation curve). This exact solution does not have the scaling form of Eq. (2). We have not been able to find a generalization of the scaling form which collapses the distribution at the critical point, but the scaling variable (typical size) must shrink exponentially as ϵ grows. One reason, why finding the scaling function may be difficult is that the system appears not to be self-averaging: the relatively good agreement between the theory and simulation shown on the right of Fig. 3 is not as true with other random number seeds, with fluctuations of an order of magnitude away from the theory. (The average over many seeds does agree with the calculated form.) While there is no scaling form solution to Eq. (5) for $\gamma=0$, we have found a family of formal, nonnormalizable solutions of the form $c(V,\epsilon)=e^{-(1+2/\beta)\epsilon}V^{\beta}$.

C. Misorientation scaling

To study the misorientation angles, we need a formula for the misorientation angle θ. Imagine a cell boundary as in Fig. 4. The rotation $R_L R_R^{-1}$ takes the crystalline axes of right-hand cell to the orientation on the left-hand side of the boundary. As before, we can write this rotation as $\exp(\mathbf{n}\cdot\mathbf{J})$, and correspondingly write R_L and R_R in terms of $\mathbf{n}_L$ and $\mathbf{n}_R$. Because the rotation angles are small across cell boundaries, $\mathbf{n}\simeq\mathbf{n}_L-\mathbf{n}_R$. The misorientation angle is

$$\mathrm{Tr}(R_L R_R^{-1})=1+2\cos\theta\simeq 3-\theta^2=3-\mathbf{n}^2,$$

$$\theta\simeq\sqrt{n_1^2+n_2^2+n_3^2}=|\mathbf{n}|. \tag{8}$$

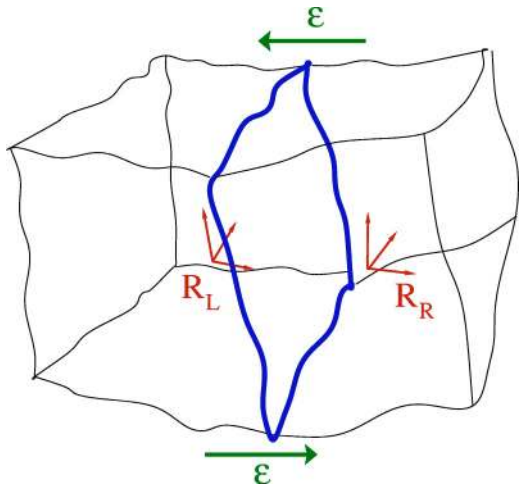

FIG. 4. Geometry of a cell boundary.

Define $\Xi(\mathbf{n})d^3n$ to be the area of cell-boundary with misorientation matrix $R=\exp(\mathbf{n}\cdot\mathbf{J})$. Since this distribution for our model is symmetric under rotations, $\Xi(\mathbf{n})=\Xi(n)$ and Eq. (8) implies that the probability distribution for the misorientation angle

$$\rho(\theta)=\rho(|n|)=4\pi n^2\Xi(n)/A_{tot}, \tag{9}$$

where $A_{tot}=\int d^3n\,\Xi(n)$ is the total cell-boundary area. Notice that the (one-dimensional) probability density for small angles θ is $4\pi\theta^2/A_{tot}$ times the (three-dimensional) cell-boundary area at one of the rotations $\mathbf{n}$ corresponding to $\theta=|\mathbf{n}|$. This is, of course, because the number of possible rotations grows with misorientation angle, as the area of a sphere in rotation space. This has the important consequence of making $\rho(\theta)$ vanish at $\theta=0$; this reflects not some special physics that avoids small misorientation angles, but a simple geometrical fact that a small net misorientation angle demands three independent rotation angles all being small. Indeed, we will see that the experimental misorientation distribution vanishes not as θ^2 as would seem natural from Eq. (9), but as θ. We will explain this, and the corresponding cusp in $\Xi(n)$, below where we incorporate the effects of cell division, which provides a source of new boundaries at zero misorientation angle.

Figure 5 shows the misorientations we measure for our area splitting model. As for the cell sizes, the misorientations across cell walls can be averaged weighting them uniformly, by the cell wall perimeter, or by its area.

We see that the mean misorientation angle in our model grows with $\epsilon^{1/2}$, as does the experimental misorientations across the IDB boundaries. We find similar scaling for volume splitting, and roughly similar for uniform splitting dynamics; our derivation below suggests that this scaling is generic for our rotational diffusion mechanism. Hence, our model will not provide an explanation for the $\theta_{\mathrm{av}}^{(GNB)}\sim\epsilon^{2/3}$ seen for the GNB's.

Since the GNB's are, in practice, distinguished from the IDB's by the number of perpendicular cell walls impinging upon them (each GNB has typically a couple of IDB's), we tested whether separating our cell boundaries into previously split GNB analogs and unsplit IDB analogs might lead the

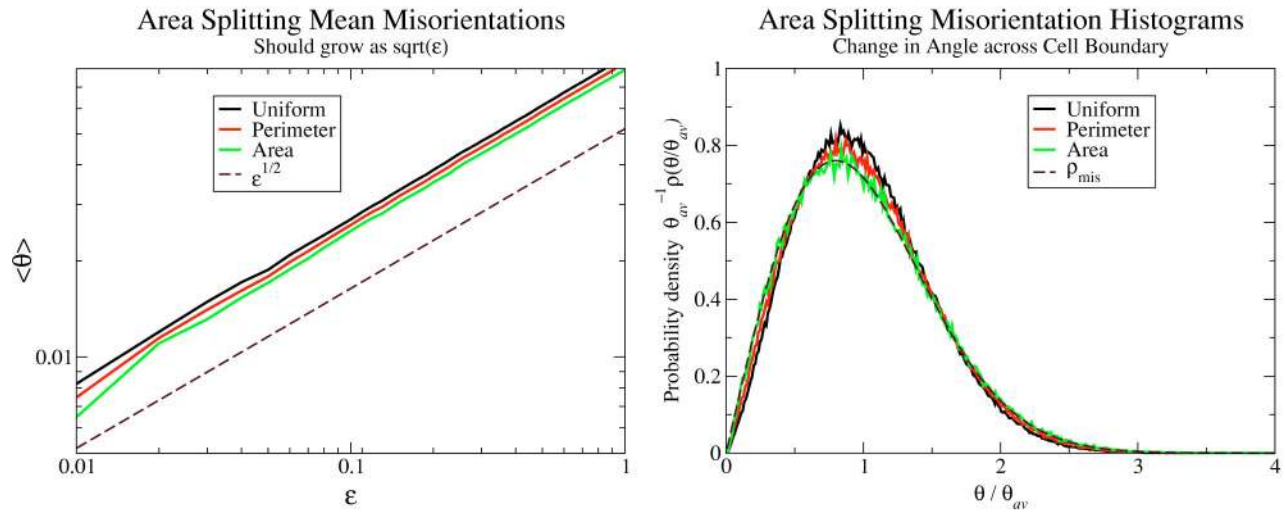

FIG. 5. Misorientation distributions: Area splitting. The misorientation angles between cell walls, weighting each equally (uniform), or weighting by perimeter or area of the cell boundary. Left: the mean misorientation angle grows as $\epsilon^{1/2}$ in our model, not only for area splitting (shown) but also for the other forms of the cell splitting rate. Right: the scaling form for the probability distribution is largely independent of the way in which one weights the cells by their size, and agrees well with the form ρ_{mis} of Eq. (14).

misorientations of the former to grow more quickly on an average with external strain. This did not occur in our model: both previously split and unsplit cell walls scale in mean misorientation with the square root of the external strain.

We can derive a simple differential equation of the time evolution of the distribution of misorientation matrices across incidental boundaries $\Xi(\mathbf{n},\epsilon)$. Since new cell boundaries are created at zero angle, the equation will be a diffusion equation with a source term:

$$\frac{\partial \Xi(\mathbf{n})}{\partial \epsilon} = 2D\nabla^2 \Xi + C\epsilon^{(1/3\gamma)-1}\delta(\mathbf{n}), \tag{10}$$

where the gradients on the right are with respect to $\mathbf{n}$, and $\delta(\mathbf{n})$ is a three-dimensional Dirac δ function (infinite at zero, zero elsewhere, integral equal to 1). The misorientation matrices diffuse with coefficient $2D$ because the two cells on either side are each diffusing with diffusion coefficient D.

The first term in Eq. (10) represents the diffusion, or random walk, in rotation space. The second term in Eq. (10) represents the creation of new cell boundaries that divide the old ones. Because we choose to weight our misorientation angle density according to the boundary area, this division does not change the cell-boundary density $\Xi(\mathbf{n})$ except at $\mathbf{n}=0$.

The new boundary area shows up in our distribution at zero misorientation angle $\delta(\mathbf{n})$. To derive the amount of new boundary area that is created per unit strain, we use a simple scaling argument. Note that the cell sizes scale as $L \sim \epsilon^{-1/3\gamma}$. The total boundary area A_{tot} will scale as the number of boundaries $1/L^3$ times the area per boundary L^2, hence as $\epsilon^{1/3\gamma}$. The new boundary area needed per unit increment of ϵ thus scales as $\epsilon^{(1/3\gamma)-1}$, giving the prefactor for the δ function in Eq. (10).

We now specialize to $\gamma=2/3$ corresponding to area splitting. If we start with no cell-boundaries at $\epsilon=0$, then the solution to Eq. (10) is

$$\Xi(\mathbf{n}) = \int_0^{\epsilon} du C u^{-1/2} \exp[-\mathbf{n}^2/8D(\epsilon-u)]/[8\pi D(\epsilon-u)]^{3/2}$$
$$= C\exp(-\mathbf{n}^2/8D\epsilon)/(8\pi Dn\sqrt{\epsilon}). \tag{11}$$

[The cell boundaries which are formed at deformation u have spread out into a Gaussian of variance $D(\epsilon-u)$]. The total boundary area $A_{tot}=2C\sqrt{\epsilon}$, as desired. This leads to a prediction for the probability distribution of misorientation angles that yields the scaling collapse (1)

$$\rho(\theta,\epsilon) = \theta_{av}^{-1}\rho_{\mathrm{mis}}(\theta/\theta_{av}) = \theta\exp(-\theta^2/8D\epsilon)/4D\epsilon, \tag{12}$$

where

$$\theta_{av} = \sqrt{2\pi D\epsilon} \tag{13}$$

and

$$\rho_{\mathrm{mis}}(x) = (\pi x/2)\exp(-\pi x^2/4). \tag{14}$$

(As we will discuss in the Appendix, this happens to be the distribution as derived by Pantleon[11,12] in a model without cell refinement.) As shown on the right in Fig. 5, this scaling form describes the simulation well: the simple scaling argument for the source term of new boundaries (above) captured the behavior of the stochastic simulation.

One can see from Fig. 6 that the predicted form is also quite a good description of the experimental data. This particular functional form is derived using $L\sim\epsilon^{-1/2}$, but the particular exponent is not crucial to the analysis: the solution for $L\sim\epsilon^{-1/3\gamma}$ has this general form [with linear slope at $\theta=0$ and $\theta_{av}(\epsilon)\sim\sqrt{\epsilon}$] for other γ as well.

IV. CONCLUSION: MISSING PIECES

We believe our simple model is the explanation for the observed scaling seen in cell refinement during plastic flow,

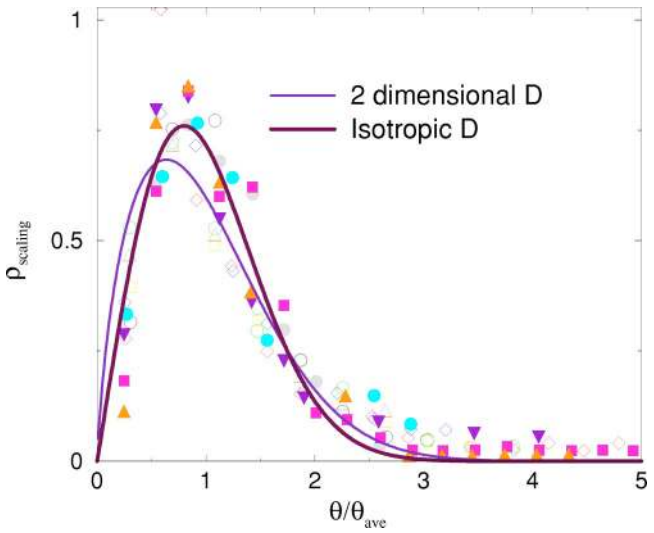

FIG. 6. Experiment vs Theories: Experimental data digitized from Hughes *et al*. (Ref. 1). The thick curve is ρ_{mis}, the scaling function of Eq. (14). The thin curve is $\rho_{\mathrm{anisotropic}}$, the solution of Eq. (A1) with a length-independent diffusion constant with one zero eigenvalue, representing a highly anisotropic rotational diffusion.

despite many missing features that are clearly relevant to the experimental behavior. In particular, we would claim that any physical system that refines by subdivision, and that undergoes random rotational distortions, is likely to enter a scaling regime similar to that seen in our model. In this section, we discuss three of the missing features and why they must be relevant for a complete engineering description.

a. *IDB/GNB distinction*. The experiments show two distinct types of cell boundaries, with different scaling exponents and scaling functions. Our model only includes one. While we get a plausible fit to the IDB scaling, the GNB misorientation angles grow faster than our rotational diffusion model can reproduce. One must note that scaling behavior in other contexts is associated with a single characteristic length scale: our model asymptotes to a morphology that is statistically unchanging at large strains except for a single rescaling of length. Because the experiments show two length scales, we expect that detailed measurements will show violations of scaling behavior, say, when the mean GNB separation length crosses the IDB separation length. Perhaps the fact that the two types of boundaries are roughly evolving on perpendicular axes allows for the approximate scaling seen.

(2) *Plastic deformation*. In our simple model, the overall plastic deformation was ignored. In a real material under compression the boundaries perpendicular to the strain axis will grow closer to one another linearly in the strain even without subdivision. Apparently[13] under the external strain the GNB's slowly rotate towards this axis, while the IDB's remain roughly aligned parallel to the axis of compression. The external strain, after this rotation is complete, will act to separate the IDB's roughly as the square root of the strain $\epsilon^{1/2}$. To get the observed refinement $\epsilon^{-1/2}$ the subdivisions must happen even faster than described by the area splitting law we focused on in the text: perimeter splitting, which in the undeformed coordinates leads to a length that scales as ϵ^{-1} would work. This begs the question of why the scaling should begin to be observed even before the rotations are complete?

Pantleon[13] suggests that this might be an explanation for the observed $\epsilon^{-2/3}$ scaling of the separation between GNB's. At short times, before the rotation is complete, the lengths vary as $\epsilon^{-1/2}$, and at long times (with the added effects of compression) they will vary faster, perhaps leading to a reasonable fit with the larger exponent.

(3) *Origins of the cell splitting, rotational diffusion*. In our model, the cell splitting and rotational diffusion are given as part of the dynamics: we do not address the physical mechanisms that produce them.

There are various proposed mechanisms for getting the cell sizes to shrink. Obviously, the cell walls cannot just move inward; the cell wall velocities would grow linearly in the system size. One could imagine a crinkling of existing cell walls (the inverse of the coarsening process seen in spinodal decomposition), or nucleating new cells at junctions of existing cell walls: neither picture is compatible with our analysis, and both involve cell wall motion that is resisted by pinned sessile dislocation junctions.[14] Subdivision as we have used it could arise from collisions between dislocations as they traverse the cell, although simple calculations suggest that the expected collision rates are too small[14,15] and do not scale correctly for our theory.[16] Cell splitting due to inhomogeneous stresses induced by neighboring cells[6] seem to us the most natural and likely mechanism. A corresponding microscopic picture would involve regions in the inhomogeneously stressed cell where the dislocations slow down, or where they are more easily pinned by obstacles or other dislocations, leading to the formation of a new cell wall.

The mechanisms driving the rotations of the crystalline axes of the cells are less well understood. The crystalline axes can rotate both directly through the rotation of the material in the cell, and indirectly because of the flux of dislocations mediated by the plastic deformation. This latter effect is well studied on larger scales in the field of texture evolution, where the plastic deformation of a polycrystal often leads to a gradual alignment of their crystalline orientations. Within a single crystalline grain, this texture evolution will on average rotate all the cells together: because the relative angles between cells is small, they will largely rotate in the same direction. One should note that the traditional explanation for the origin of the GNB's indicates that their misorientation angles could well have a overall mean drift in addition to the random diffusion. It is said that GNB's are observed to have rotational misorientations that alternate in sign, because they separate regions with differing active slip systems;[4] the combination of the differing plastic strains and rotations in neighboring pairs of cells can equal the net imposed plastic deformation. In this picture, the net rotation angles across the GNB's [Eq. (4)] should have a mean drift term in addition to the diffusion term.

ACKNOWLEDGMENTS

This work was supported by the Digital Material Project No. NSF KDI-9873214, the ITR/ASP Project No.

NSF ACI0085969, and the Harvard Society of Fellows. We thank Paul Dawson and Ali Argon for useful conversations, Karin Dahmen for help with the manuscript, and Wolfgang Pantleon and Darcy Hughes for constructive criticism.

APPENDIX: CONNECTIONS WITH STOCHASTIC DISLOCATION THEORIES

The distribution for the misorientation angle for the simple rotational diffusion model, $\rho_{\mathrm{mis}}(x)$, happens to have the same form as one derived by Pantleon[11,12] without considering cell refinement, and by assuming that the noise in the cell orientations was due to random, uncorrelated fluctuations in the dislocation flux. It behooves us, therefore, to discuss how Pantleon's work can be interpreted in our context.

Pantleon's theory, also suggested by Nabarro,[17] and Argon and Haasen,[15] is that the stochastic noise in the flux of dislocation from either side of the cell boundary leads to randomness in the evolution of the cell-boundary angles. Each dislocation passing through a cell, say, may shift the top plane of atoms by a distance b with respect to the bottom plane, where b is the Burgers vector of the dislocation (roughly the lattice constant). The crystalline axes within a cell of characteristic height L will rotate due to one dislocation an amount proportional to b/L. Under a strain increment $\Delta\epsilon$, a cell of characteristic height L must have $N=L\Delta\epsilon/b$ dislocations impinging on the side cell boundary. A roughly equal and opposite average flux will impinge on the cell boundary from the cell on the other side. If the dislocations move independently (which we will argue does not occur), then one expects that there will be a net residue after the strain increment of roughly $\sqrt{N}=\sqrt{L\Delta\epsilon/b}$. Hence, the predicted drift in angle after a strain increment of $\Delta\epsilon$ is $\Delta\theta = \sqrt{N}b/L=\sqrt{b\Delta\epsilon/L}$. The diffusion constant is given by $D(L)\sim(\Delta\theta)^2/\Delta\epsilon\sim b/L$. Because a single dislocation produces a larger net rotation for smaller cell, the stepsize in the random walk in rotation space becomes larger as our cells get smaller.

Pantleon and Hansen[5] consider three cases, where one, two, and three slip systems are activated. The geometry of a given cell—the direction and strength of the applied shear with respect to the crystalline axes—will determine what types of dislocations are allowed to pass through the cell. If only one slip system is active, the rotation of the cell will be confined to a single axis. In our formulation, the diffusion constant in rotation space will be anisotropic: in this case, it will be a rank 1 tensor (a 3×3 matrix with only one nonzero eigenvalue). Two slip systems will give a rank 2 tensor, with one zero eigenvalue. Three slip systems will allow the cell to diffuse in any direction, but even so the diffusion constant D will, in general, be anisotropic.

To make contact with Pantleon, we consider a more general evolution law for the misorientation in area splitting:

$$\frac{\partial\Xi(n)}{\partial\epsilon}=D_{ij}(L)\nabla_i\nabla_j\Xi+C\epsilon^{1/2}\delta(n). \qquad \text{(A1)}$$

Here, we have allowed for an anisotropic, cell-size-dependent diffusion constant by introducing the symmetric tensor $D_{ij}(L)$ depending on the current cell size L. The symmetric diffusion tensor D_{ij} will vary with the geometry of the particular cell boundary: it can depend both on the relative orientation of the crystal and the strain tensor with respect to the plane of the cell boundary. We will first consider the anisotropy while ignoring the refinement [$D_{ij}(L)$ independent of L], in analogy to previous work, and then incorporate the refinement [$D_{ij}(L)$ proportional to $1/L\sim\epsilon^{1/2}$ as argued above].

Pantleon[5,11,12] in most of his analysis ignores cell refinement. If we make D_{ij} independent of L and set $C=0$ in Eq. (A1), we get an anisotropic diffusion equation whose solution (assuming a narrow initial distribution of misorientations) is an anisotropic Gaussian with variances given by the inverse eigenvalues of D, with the experimentally observed scaling $\theta_{av}\sim\epsilon^{1/2}$. If we assume D has one nonzero eigenvalue, we get the Gaussian distribution derived by Pantleon and Hansen for one active slip system. If we assume D has two equal, nonzero eigenvalues, we get the Rayleigh distribution that they find for two perpendicular systems of edge dislocations [which, coincidentally, is the same distribution that we found above (14) with an isotropic D and a source term]. If we assume D is isotropic, we get the Maxwell distribution they find for three perpendicular systems of dislocations.

What happens to the solution of Eq. (A1) when we incorporate cell refinement? Pantleon[12] notices that nonconstant cell size must change the scaling of average angle with strain. By setting $D(L)\sim\epsilon^{1/2}$ in accordance with Ref. 2, and changing variables to $\tau=\epsilon^{3/2}$ in Eq. (A1), we can map it into a problem quite similar to Eq. (10) except that the source term is of magnitude proportional to $\tau^{-2/3}$. The solution to this equation has a shape quite similar to that shown in Fig. 6, but with an average angle $\theta_{av}\sim\sqrt{\tau}\sim\epsilon^{3/4}$. This yields a 3/4 power of the strain incompatible with the scaling observed for the incidental cell boundaries. Pantleon is aware of this:[12] in an analogous calculation he gets $\theta_{av}\sim\epsilon^{0.72}$.

(If we abandon dislocation noise as the origin of the rotational diffusion, and take the crystalline lattice orientations as our basic variables, then there are no microscopic lengths remaining in the problem. The diffusion constant then naturally depends only on the local geometry of the cell boundary, and hence is independent of the length scale.)

The key to the discrepancy is, of course, that the dislocations motion is not uncorrelated; they must be moving in a collective manner. The interaction energy between dislocations is large, and diverges logarithmically with distance, reflecting the infinite stiffness of a crystal to gradients in the axes of rotation. In early stages of hardening, one might plausibly argue that the dislocations are sufficiently far apart that their interaction forces do not dominate. But in the regime studied here, the fact that the dislocations organize into boundaries (avoiding rotational distortions within the cells) is a clear signal that it is no longer sensible to treat their evolution independently. If the top half of a cell boundary received more dislocations from the right-hand cell than the bottom half, this would produce an enormous bending force

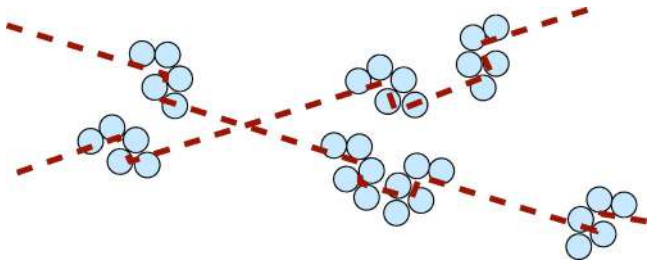

FIG. 7. Correlated atomic rearrangements associated with simple dislocation motion.

on the cell. Such an event could only happen for reasonable energy cost if this bending were screened by the division of the cell by a new boundary.

The stochastic dislocation flux models will be generally applicable whenever the correlations between their motions vanish at distances comparable to the cell sizes. Our model is correct in the other limit: our cells only rotate as units. Thus, our model is appropriate for systems where the dislocation motions are strongly correlated on the scale of the cells—so that their motion can always be described as mediating overall rotations of each cell. Both descriptions are only a starting point for a complete theory.

Consider an analogy: dislocation motion modeled as rearrangements of atoms, versus as the evolution of a continuum curve. In the atomic description (Fig. 7), one would identify characteristic atomic motions (say, kink diffusion events in the case of semiconductors), at rare sites scattered through the crystal. These sites would be strongly correlated (lying along the dislocations); their dynamics would produce unusual zipper motions (kinks diffusing along dislocations). We expect similar correlations to arise in the dislocation motions mediating cell-boundary evolution: the dislocations will form correlated dances to keep rotational gradients from entering the cells. On the other hand, treating the dislocation motion as the evolution of a continuous curve makes it difficult to incorporate the anisotropic dynamics and lattice pinning effects—our model so far has ignored the corresponding crystalline and shear anisotropies in the evolution of cell structure.

We can incorporate some of this asymmetry by hand into our model. Pantleon and Hansen[5] point out that the individual cell boundaries have rather low symmetries. The diffusion tensor in Eq. (A1) describes the evolution of that subset of cell boundaries with a particular cell-boundary orientation and (average) crystal lattice orientation with respect to the external shear. There is no reason that for a low-symmetry geometry that the diffusion constant will be isotropic, geometry dependent, or material dependent: the general evolution law is given in Eq. (A1) with D_{ij} independent of L. One must solve for the distribution at fixed geometry and then average over geometries to predict the experimental distribution (as also discussed in Sec. 5.2 of Ref. 5). If we assume a strongly anisotropic rotational diffusion tensor with one zero eigenvalue and the other two equal (corresponding roughly to Pantleon's analysis with two active slip systems) we can solve Eq. (A1) to find a scaling collapse (1) with scaling function

$$\rho_{2\mathrm{dim}}(x) = (\pi^3 x/64)\exp(-\pi^3 x^2/128) K_0(\pi^3 x^2/128), \tag{A2}$$

where K_0 is the modified Bessel function of the second kind. This scaling function is shown in Fig. 6.

It is important also to note that effects that seem clearly related to cell-boundary formation have been seen in finite-element simulations of single-crystal plasticity by Mika and Dawson *et al*.[6] Their system consisted of several crystalline grains with differing orientations, subject to an external shear. The inhomogeneous strains within the grains led to the formation of subgrain structures very similar to cells. The distribution of cell boundaries in their simulation was also found to scale, with strain dependence and functional form similar to that seen for geometrically necessary boundaries (that is, scaling with the 2/3 power of strain, and not with the 1/2 power seen for the IDB's). Hence, Dawson *et al*. find cells in a simulation totally without dislocations.

[1] D.A. Hughes, D.C. Chrzan, Q. Liu, and N. Hansen, Phys. Rev. Lett. **81**, 4664 (1998).

[2] D.A. Hughes, Q. Liu, D.C. Chrzan, and N. Hansen, Acta Mater. **45**, 105 (1997); A. Godfrey and D.A. Hughes, *ibid*. **48**, 1897 (2000).

[3] B. Bay, N. Hansen, and D. Kuhlmann-Wilsdorf, Mater. Sci. Eng., A **113**, 385 (1989).

[4] D. Hughes (private communication).

[5] W. Pantleon and N. Hansen, Acta Mater. (to be published).

[6] D.P. Mika and P.R. Dawson, Acta Mater. **47**, 1355 (1999); N. R. Barton and P. R. Dawson (unpublished).

[7] E.D. McGrady and R.M. Ziff, Phys. Rev. Lett. **58**, 892 (1987).

[8] Z. Cheng and S. Redner, Phys. Rev. Lett. **60**, 2450 (1988).

[9] P. Hähner, K. Bay, and M. Zaiser, Phys. Rev. Lett. **81**, 2470 (1998); R. Thomson and L.E. Levine, *ibid*. **81**, 3884 (1998); I. Groma and B. Bako, *ibid*. **84**, 1487 (2000).

[10] Write $\bar{V} = \int \rho_{\mathrm{vol}}(V) dV$, use Eq. (2) to compute $\partial \bar{V}/\partial \sigma$, change variables to $y = V/\bar{V}$, and substitute in the scaling form Eq. (2).

[11] W. Pantleon, Scr. Mater. **35**, 511 (1996).

[12] W. Pantleon, Acta Mater. **46**, 451 (1998).

[13] W. Pantleon (private communication).

[14] F. Prinz and A.S. Argon, Phys. Status Solidi B **57**, 741 (1980). They discuss not collisions between dislocations on different slip systems, but mutual trapping of dislocations with opposite Burgers vector on one slip system: our analysis still applies. One should note that Argon now believes that cell boundaries may move during plastic deformation through avalanches of failures of these sessile dislocation junctions.

[15] A.S. Argon and P. Haasen, Acta Metall. Mater. **41**, 3289 (1993), Eq. (21).

[16] J.P. Sethna and E. Demler, cond-mat/0104552 (unpublished).

[17] F.R.N. Nabarro, Scr. Metall. Mater. **30**, 1085 (1994).